Multi-approach Gravity Field Models from Swarm GPS data

Swarm models validation

Delft University of Technology (TU Delft)
Astronomical Institute of the University of Bern (AIUB)
Astronomical Institute Ondřejov (ASU)
Institute of Geodesy Graz (IfG)
Ohio State University (OSU)

Version 1
2019-04-11

Prepared and checked:		Approved:	
João Encarnação Work Package Manager	2019-04-11	Pieter Visser Project Manager	2019-04-11

Contents

List of Figures

List of Tables

1 Version history

Version 0.1, 2018-08-16

- Validation of combined models, version 06.

Version 0.2, 2018-11-19

- Validation of individual models (only);
- Analysis done up to degree and order 20 (instead of 40);
- Plotting Equivalent Water Height (instead of Geoid height);
- Complete GRACE time series considered (until June 2017).

Version 0.3, 2018-12-19

- Validation of individual models (only);
- Analysis done up to degree and order 20 (instead of 40);
- Plotting Equivalent Water Height (instead of Geoid height);
- Complete GRACE time series considered (until June 2017).

Version 1, 2019-02-17

- Validation of combined models, version 07 to 10;
- The GRACE solutions are smoothed to 300km to limit the suppression of geophysical signal;
- Updated the last 7 months of GRACE, following processing developments at Center for Space Research (CSR);
- discarded first half of 2014 to make validation fair regarding the different combination strategies.

2 Introduction

This report validates the combined GFMs produced on the context of the *Multi-approach Gravity Field Models from Swarm GPS data* project. The approach for combining individual gravity field solutions, i.e. those produced by the various partners mentioned in Section 3, is described in Section 4.1. The validation of the combined models is described in Section 4.2. Finally, the analysis results are presented in Section 5.

3 Source data

The individual gravity field solutions are produced by the institutes listed in Table 1.

Inst.	Approach	Reference
AIUB	Celestial Mechanics Approach (CMA) (Beutler et al. 2010)	Jäggi et al. (2016)
ASU	Decorrelated Acceleration Approach (DAA) (Bezděk et al. 2014; Bezděk et al. 2016)	Bezděk et al. (2016)
IfG	Short-Arcs Approach (SAA) (Mayer-Gürr 2006)	Zehentner and Mayer-Gürr (2016)
OSU	Improved Energy Balance Approach (IEBA) (Shang et al. 2015)	Guo et al. (2015)

Table 1 – Overview of the gravity field estimation approaches

Additional details about the different gravity field approaches can be found in (Teixeira Encarnação and Visser, 2017).

The version of the individual GFMs is listed in Table 2.

Gravity Field Model	version	Kinematic Orbit
AIUB	01	AIUB
ASU	02	IfG
IfG	03 – 06	IfG
OSU	02	AIUB
combined	07	N/A
combined	08	N/A
combined	09	N/A
combined	10	N/A

Table 2 – Versions of the GFMs, and the KOs used in their estimation, relevant to this report.

The version numbers listed in Table 2 are relevant within the project and are reported so that it is possible to trace back the results presented in Section 5. Particular to the combined models, versions 07 to 10 relates to the latest combination strategy, further described in Section 4.1.

4 Methodology

4.1 Combination

We analyse the combination of the monthly gravity fields from the different analysis centres on the basis of two approaches: one at the level of the solutions considering weights derived from

Variance Component Estimation (VCE) and another at the level of Normal Equation (NEQ). The combination at the NEQ level includes two steps:

1. determination and application of empirical factors to limit the effect of the different types of formal errors,
2. application of the relative weights derived by VCE at the solution level (i.e. without considering NEQ).

The empirical factors are necessary because the formal errors of the individual contributions are impaired by analysis errors (from the diverse background models, accumulated during integration and exacerbated by algorithmic differences), and do not necessarily represent the actual error levels of the monthly gravity fields resulting solely from observation noise. Consequently, the scale of the formal errors is incompatible between the various individual solutions and the empirical weights calibrate them towards a common scale. The empirical factors were determined by the study of pairwise combinations (Meyer, Jean and Jäggi, 2018) for each month separately. This necessary step leading up to the NEQ-level combination is a robust approach as demonstrated in the frame of the European Gravity Service for Improved Emergency Management (EGSIEM) project (Jäggi et al., 2018).

Both approaches consider the complete degree range (degrees 2 to 40). On top of these two strategies we test the combination variants where the VCE weights and/or empirical factors are determined taking degrees 2 to 20 into account, thus resulting in a total of four different combination strategies. The latter variant, where only degrees 2 to 20 are considered when deriving the weights/factors, is designed to test the hypothesis that the different types of formal errors in the individual solutions manifest themselves more intensively at the 21 to 40 degree range, thus potentially introducing larger biases in the resulting combination. In principle, these biases are better handled with the empirical factors but it is not always practical (or possible) to derive their values without adding additional assumption-based biases or properly taking into account their different spectral properties, such as the different ratios between the low (2-20) and high (21-40) formal errors of the various individual solutions.

Table 3 connects the version numbers to the combination strategies described above.

version	VCE weights	empirical factors	combination level	short name
07	2-20	2-20	NEQs	*NEQ comb 20*
08	2-40	2-40	NEQs	*NEQ comb 40*
09	2-20	N/A	solution	*VCE comb 20*
10	2-40	N/A	solution	*VCE comb 40*

Table 3 – Versions of the combined GFMs, described in terms of the corresponding combination strategy.

Unlike earlier versions of the combination, all four strategies take relative weights determined by VCE (on solution level) into account. This is now feasible because there are two time-series based on AIUB orbits (i.e. AIUB and OSU) and two time-series based on IfG orbits (i.e. IfG and ASU). Therefore the impact of the KOs on the solutions and on the VCE weights is balanced. This step had to be omitted in earlier versions, because there where only three time-series available for combination.

It should be noted that, other than in the case of AIUB, ASU and IfG, the formal errors of OSU's solutions do not represent the changes in quality related to the increase in the GPS observation sampling rate, before July 2014. As a result of the unreasonably large empirical factors associated with the OSU solutions (coming from the previously mentioned comparatively low formal errors), it was impossible to converge the combination at the level of NEQ considering VCE weights and empirical factors derived from the complete degree range, version 08 (*NEQ comb 40*). The only possibility would be to relax the empirical weights beyond the search radius considered in the remaining combination variants and unrealistically bias the result towards OSU's individual solutions, largely eliminating the contribution from the remaining three individual solutions. For this reason, the analysis does not include the December 2013 and the first half of 2014.

4.2 Validation

The validation is done by comparing the individual and combined solutions to the Release 6 (RL06) GRACE GFMs produced at CSR.

So that the geophysical signal contained in the Swarm solutions is seen clearly, all solutions undergo a 750km radius spherical cap Gaussian filtering, unless otherwise noted. The GRACE solutions are smoothed only at 300km radius spherical cap in order to better preserve the geophysical signal, which is of significant amplitude up to degree 30/40. If the smoothing radius used for Swarm is applied to GRACE, the amplitude of the geophysical signal in the latter is greatly reduced; this would have been seen in the regional analysis of Section 5.3 as a consistently lower amplitude of the GRACE time series.

Some analyses are restricted to either the land or ocean areas. In those cases, the land or ocean mask is applied in the spatial domain and a Spherical Harmonic (SH) analysis is done on the masked grid. The $C_{2,0}$ coefficient in all solutions has been replaced by the values provided in Cheng and Ries (2016). The GRACE Gravity Model 05 (GGM05G) (Tapley et al. 2013) static GFM is subtracted from all models in order to isolate the time-variable component of Earth's gravity field. We chose to show the gravity field in terms of EWH, except for the statistics related to the correlation coefficient, which are non-dimensional as usual. Both GRACE and Swarm gravity field time series are linearly interpolated to a common time domain defined by the middle epoch of the GRACE solutions and the mid-month epoch of the Swarm solutions. The aforementioned issue with the influence of the formal errors of the OSU solutions on *NEQ comb 40* dictated that the first half of 2014 had to be discarded. Therefore, the analysis spans all available months common to GRACE and Swarm, i.e. between July 2014 and June 2017.

5 Results

The analysis is split into a spatial and temporal validation. The former focuses on the consistency of the solutions independently at each month, while the latter determines how the temporal variations in the Swarm solutions correlate with what the GRACE time series describes.

5.1 Spatial analysis

Figure 1 illustrates (an estimate of) the average quality of the various Swarm solutions in the spectral domain (top) and the cumulative degree-mean temporal RMS difference (bottom). It is computed as average of the complete data period of the degree-RMS of the difference between Swarm and GRACE GFMs, considering 750km and 300km Gaussian smoothing, respectively. The degree amplitudes remain relatively constant with increasing degree, instead of growing in terms of EWH, as the result of the smoothing.

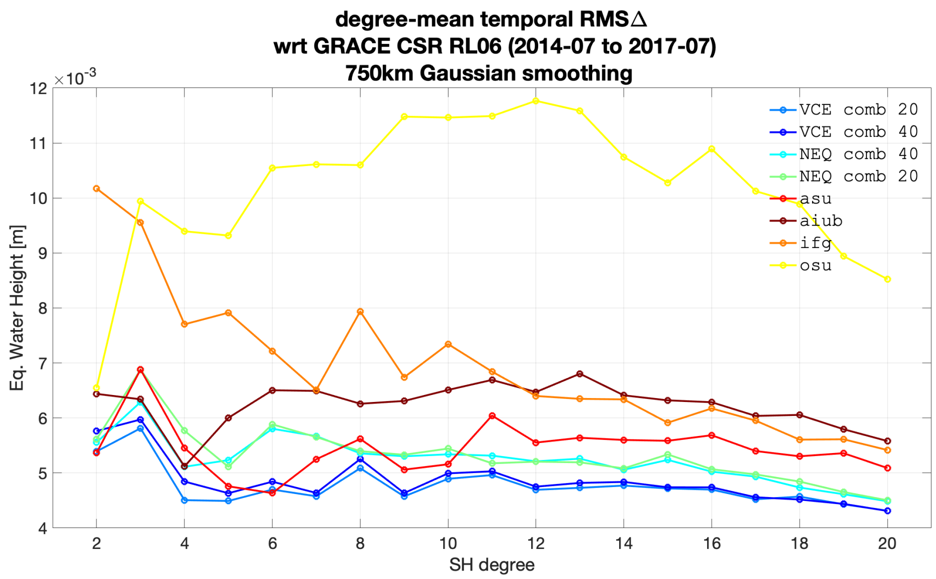

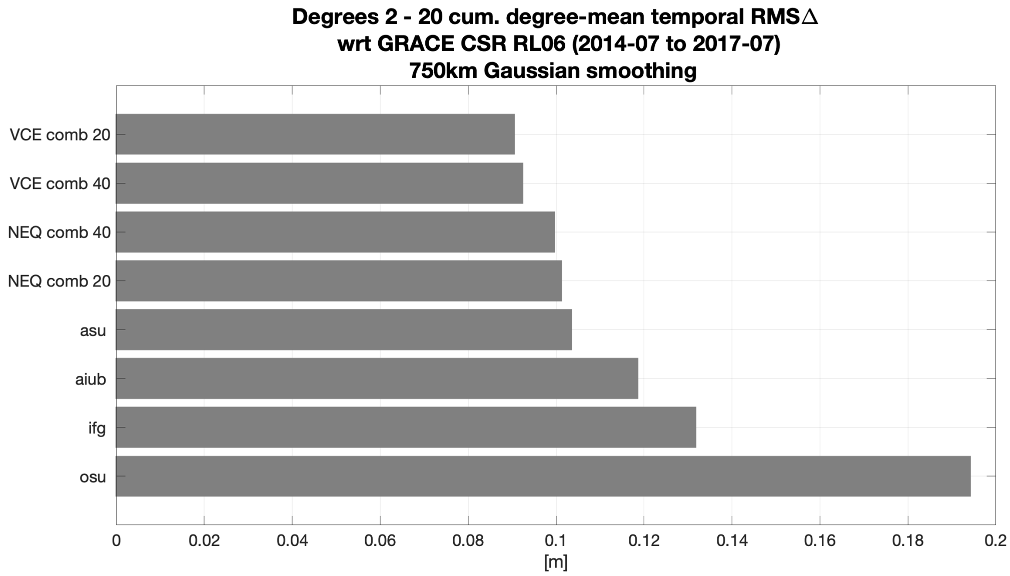

Figure 1 – Per-degree mean of the RMS difference (top) and cumulative degree-mean temporal RMS difference (bottom) between the Swarm and GRACE GFMs, considering 750km and 300km Gaussian smoothing, respectively.

The legend at the top line plot is sorted in order of increasing cumulative degree-mean temporal RMS difference, with this value plotted in the bar plot at the bottom. Figure 1 confirms that all combination strategies perform better than any individual solution, with the solution-level combination being closer to GRACE than the NEQ counterpart. In other words, none of the yellow (OSU), orange (IfG), brown (AIUB) or red (ASU) lines are persistently below the combined solutions.

Figure 2 gives an overview of (an estimate of) the evolution of the quality of the various Swarm solutions over time (top) and its global sum (bottom). This measure of quality is computed for every month as the cumulative degree-RMS of the difference between Swarm and GRACE GFMs, exclusively over land areas, considering 750km and 300km Gaussian smoothing, respectively.

The main pattern in Figure 2 is that all solutions tend to have comparable errors with time,

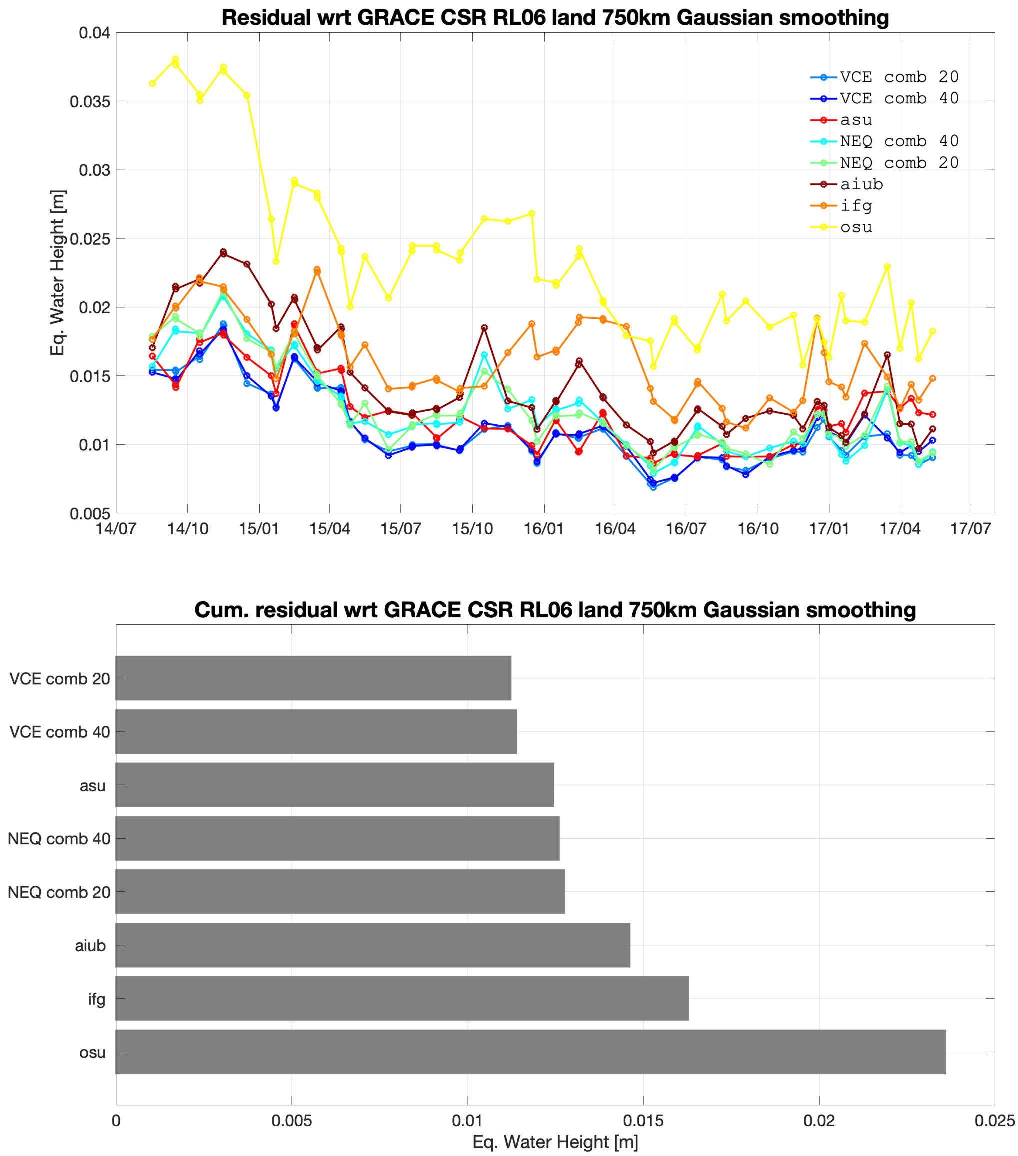

Figure 2 – Epoch-wise cumulative spatial RMS (top) and its global sum (bottom) of the difference between Swarm and GRACE GFMs, over land areas, considering 750km and 300km Gaussian smoothing, respectively.

except for OSU, generally having higher errors. There are periods of high errors (e.g. 2014) that generally produce less accurate solutions. These periods are attributed to higher solar activity, which amplifies the intensity and frequency of ionospheric scintillations, to which the Swarm data is particularly sensitive (Jäggi et al., 2016). The NEQ-level combinations differ from GRACE at a (slightly) higher overall level than the ASU solution (bottom plot), thus indicating that this combination variant is sub-optimal, considering the spatial RMS difference w.r.t. GRACE as a metric for optimality.

Figure 3 quantifies the epoch-wise variability of the GFMs over the oceans (top) and its global sum (bottom), considering 750km and 300km Gaussian smoothing for Swarm and GRACE GFMs, respectively.

Comparing the EWH amplitudes between Figure 2 and Figure 3, those related to the ocean areas are roughly 50% larger than those related to the land areas. We interpret this observation

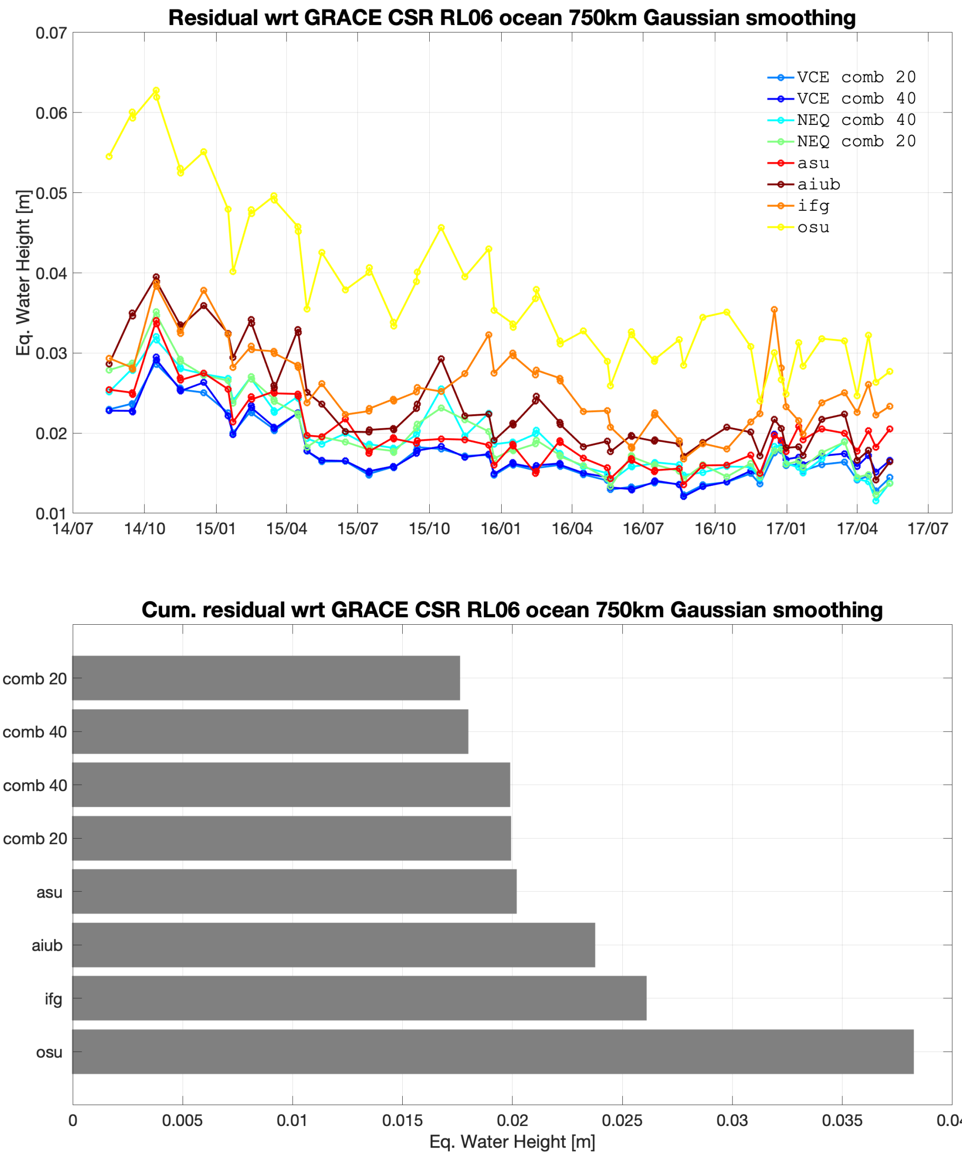

Figure 3 – Epoch-wise cumulative spatial RMS (top) and its global sum (bottom) of the difference between Swarm and GRACE GFMs, over ocean areas, considering 750km and 300km Gaussian smoothing, respectively.

as indication that Swarm does not have sufficient accuracy to resolve oceanic mass transport processes, since the gravity field variations over the ocean are of small amplitude and would require accuracy comparable to GRACE to resolved them.

5.2 Temporal analysis

Figure 4 illustrates how the Swarm solutions correlate in time with GRACE over land areas. The quantity shown is the per-degree average of the temporal correlation coefficient (top) and its sum over the entire degree range (bottom) between the Swarm and GRACE solutions. In other words, the temporal correlation at every Stokes coefficient is computed and the average over each degree is plotted at the top.

It is clear that the Swarm solutions have the highest temporal correlation with GRACE at

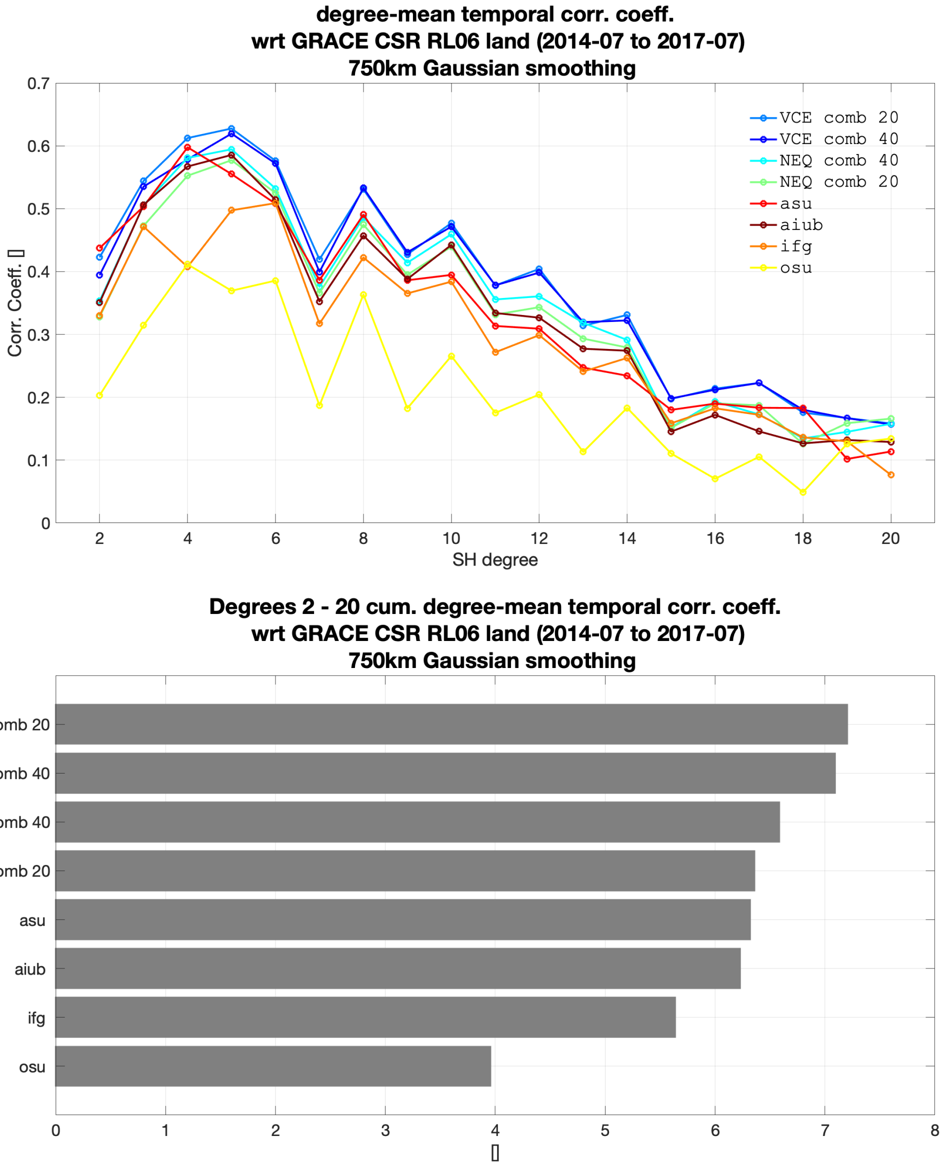

Figure 4 – Per-degree mean (top) and its overall cumulative (bottom) of the correlation coefficient between Swarm and GRACE GFMs, over land areas, considering 750km and 300km Gaussian smoothing, respectively.

degrees 2 to 10, dropping to roughly 0.1 at degree 16. In other words, the signal content of the Swarm solutions is certainly restricted to degrees below 15.

OSU's solutions generally correlate the lowest with GRACE. The velocity measurements, which are needed for energy balance approaches, are unavailable from the kinematic orbits. The tedious data filtering and processing to approximate velocity errors is still imperfect, particularly in light of the spurious jumps in most of the kinematic orbits even in the cases without the GPS tracking signal degradations from the Southern Atlantic anomalies. In spite of this, there is clearly a region of constructive correlation for degrees below 10 that is beneficial to the combination. This statement is motivated by the fact that, albeit this solution stands out as having the largest discrepancies w.r.t. GRACE, the combined models do not suffer any meaningful degradation, which would be the case if they contained little or no physical information.

Figure 5 illustrates how the Swarm solutions correlate in time with GRACE over ocean areas.

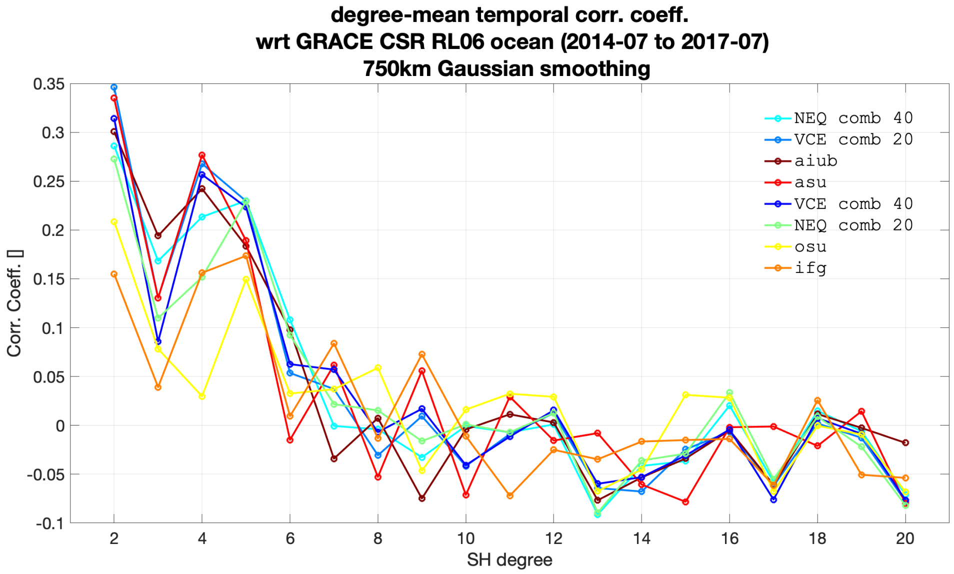

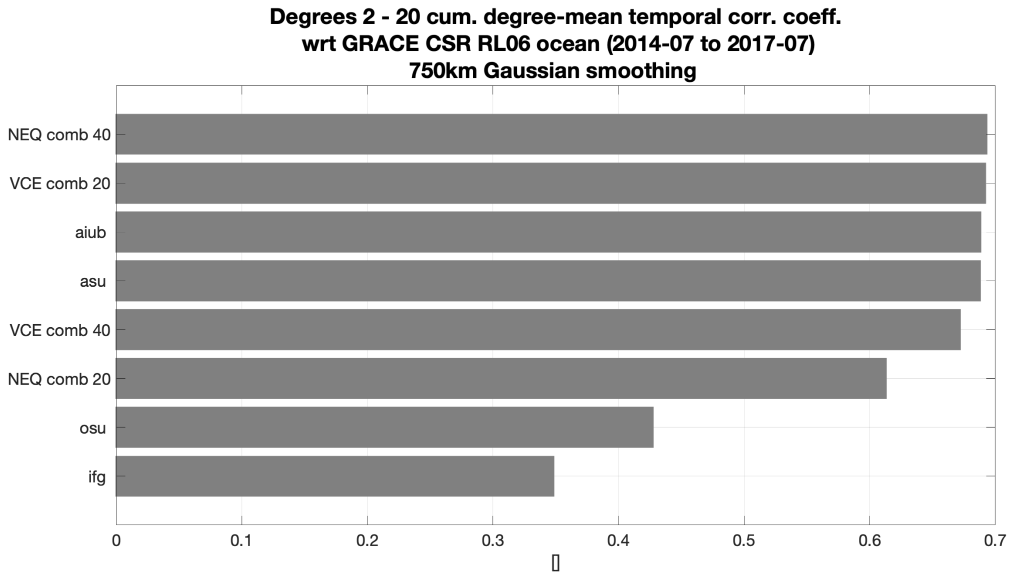

Figure 5 – Per-degree mean (top) and its overall cumulative (bottom) of the correlation coefficient between Swarm and GRACE GFMs, over ocean areas, considering 750km and 300km Gaussian smoothing, respectively,

Over the oceans, there is very little temporal agreement with GRACE, with a correlation coefficient no higher than 0.35, vanishing at degrees 6 and above; degree 3 generally is particular poorly correlated compared to neighbouring coefficients. Note that it is not possible to derive a definitive interpretation from degree 2 since the $C_{2,0}$ coefficient has been artificially replaced. The cumulative degree mean temporal correlation reinforces the little temporal agreement between Swarm and GRACE over the oceans, with cumulative values an order of magnitude lower than the land counterparts.

5.3 Time series of storage catchments

The geophysical signal represented by the Swarm solutions is now evaluated on the basis of the time series of average EWH over restricted geographical locations, see Figure 6. Each averaging is done over the corresponding spatial truncation of an equiangular grid representation of the SH coefficients. Similar maps for the Swarm models are shown in Section 5.4. The locations shown in Sections 5.3.1 to 5.3.18 are related to the largest hydrological basins and polar regions with the highest signal variability observed by GRACE.

We perform a parametric regression on all time series considering a constant and drift terms, along with annual and semi-annual sine and cosine terms to improve the robustness. We plot the linear part of this regression, in order to quantify the accuracy of Swarm-derived climatological trends.

The GRACE models were smoothed with a Gaussian kernel with 300km radius, less aggressive than the smoothing applied to the Swarm models, in order to preserve the geophysical signal in the former solutions. This discrepancy in smoothing radius is needed, otherwise the amplitudes of the time series derived from GRACE and Swarm would be in much less agreement (not shown). Furthermore, there is no effort to meticulously consider or implement proper leakage reduction methods, e.g., by Guo, Duan and Shum (2010).

The time series are plotted along with tables presenting some statistics. The values of the constant and linear terms for the Swarm and GRACE solutions (column 1) are show in terms of EWH (columns 2 and 4). Additionally, the difference of these parameters between the various Swarm solutions and GRACE is listed in columns 3 and 5 (the values for GRACE in these columns is zero). Finally, the correlation coefficients between the Swarm solutions and GRACE is presented in the last column (the value for GRACE is 1).

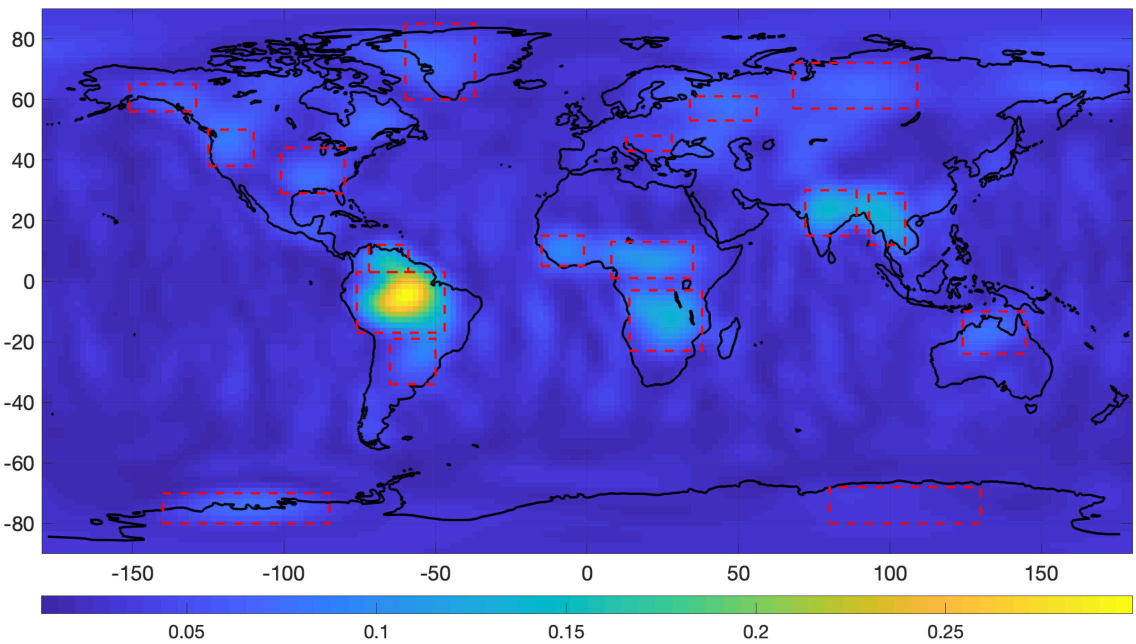

Figure 6 – Temporal variability of the GRACE models, including the boundaries of the regions analysed in Section 5.3.1 to Section 5.3.18.

5.3.1 Amazon basin

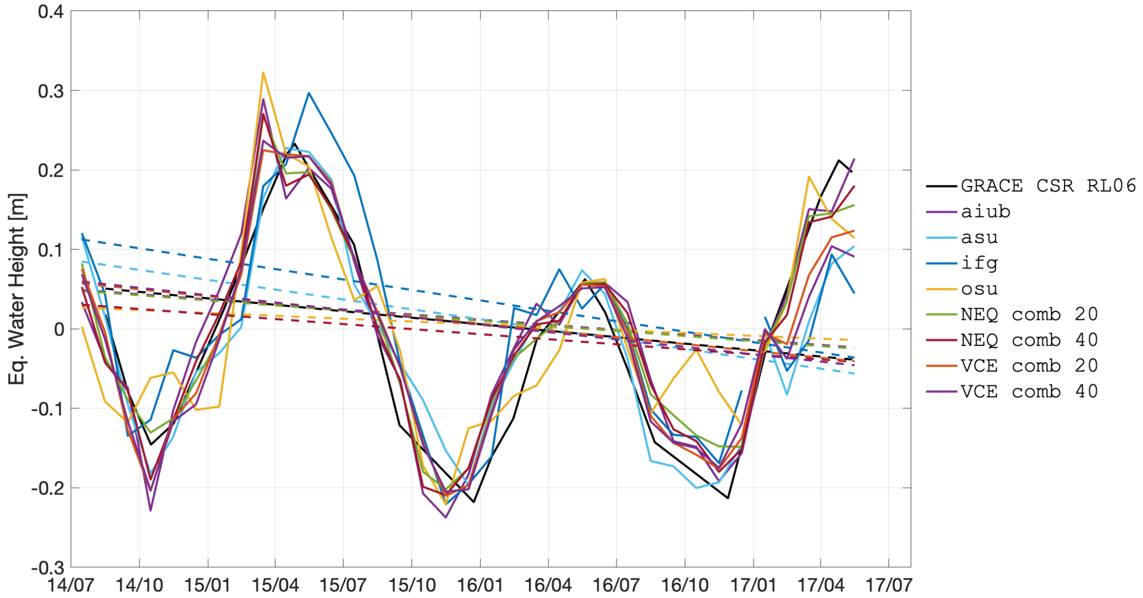

Figure 7 – Time series of EWH for the Amazon basin (latitude -17 to 3 degrees, longitude -76 to -47 degrees).

solution	constant term [cm]	constant term Δ [cm]	linear term [cm/y]	linear term Δ [cm/year]	corr. coeff. [ ]
GRACE CSR RL06	-0.6	0.0	-3.3	0.0	1.00
aiub	0.9	1.5	-2.6	0.7	0.93
asu	-1.2	-0.6	-5.0	-1.7	0.93
ifg	1.0	1.6	-5.2	-2.0	0.86
osu	-0.1	0.5	-1.4	1.8	0.87
NEQ comb 20	0.7	1.3	-2.6	0.7	0.95
NEQ comb 40	3.5	4.0	-2.5	0.7	0.94
VCE comb 20	0.3	0.9	-3.4	-0.2	0.94
VCE comb 40	0.1	0.7	-3.7	-0.5	0.93

Table 4 – Statistics of the agreement between the GRACE and Swarm time series for the Amazon basin.

5.3.2 Orinoco basin

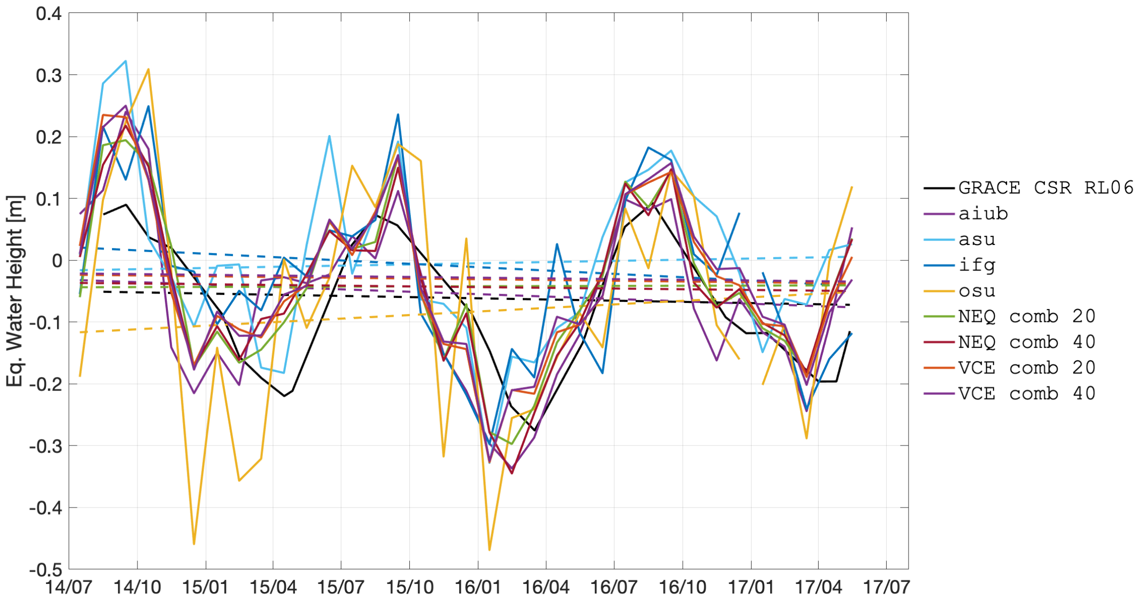

Figure 8 – Time series of EWH for the Orinoco basin (latitude -3 to 12 degrees, longitude -72 to -59 degrees).

solution	constant term [cm]	constant term Δ [cm]	linear term [cm/y]	linear term Δ [cm/year]	corr. coeff. [ ]
GRACE CSR RL06	-6.4	0.0	-0.8	0.0	1.00
aiub	-5.7	0.8	-1.6	-0.8	0.72
asu	-0.1	6.3	0.8	1.5	0.77
ifg	-2.2	4.3	-2.2	-1.4	0.72
osu	-7.2	-0.7	2.3	3.1	0.67
NEQ comb 20	-4.2	2.2	0.1	0.9	0.85
NEQ comb 40	-3.6	2.8	-0.5	0.3	0.82
VCE comb 20	-3.1	3.3	-0.5	0.3	0.81
VCE comb 40	-2.9	3.6	-0.5	0.3	0.82

Table 5 – Statistics of the agreement between the GRACE and Swarm time series for the Orinoco basin.

5.3.3 La Plata basin

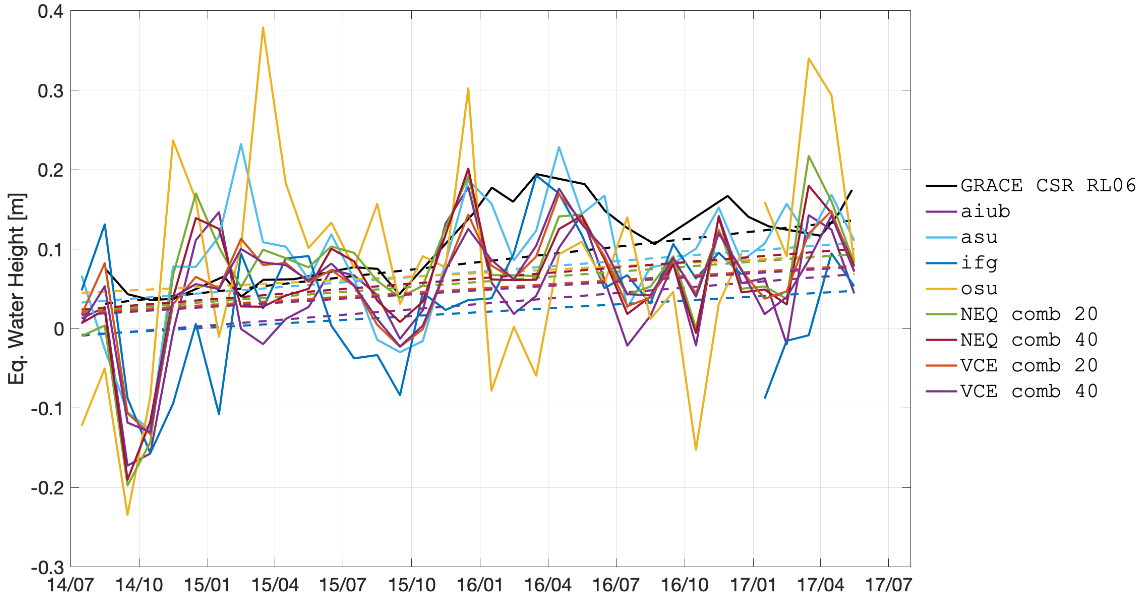

Figure 9 – Time series of EWH for the La Plata basin (latitude -34 to -19 degrees, longitude -65 to -50 degrees).

solution	constant term [cm]	constant term Δ [cm]	linear term [cm/y]	linear term Δ [cm/year]	corr. coeff. [ ]
GRACE CSR RL06	9.8	0.0	3.8	0.0	1.00
aiub	3.4	-6.3	2.7	-1.1	0.58
asu	8.5	-1.3	2.7	-1.2	0.50
ifg	3.0	-6.8	2.0	-1.9	0.58
osu	7.8	-2.0	1.7	-2.1	-0.03
NEQ comb 20	6.2	-3.6	2.5	-1.3	0.45
NEQ comb 40	2.0	-7.8	2.7	-1.1	0.56
VCE comb 20	5.3	-4.5	2.1	-1.7	0.54
VCE comb 40	5.1	-4.7	2.1	-1.7	0.58

Table 6 – Statistics of the agreement between the GRACE and Swarm time series for the La Plata basin.

5.3.4 Mississippi basin

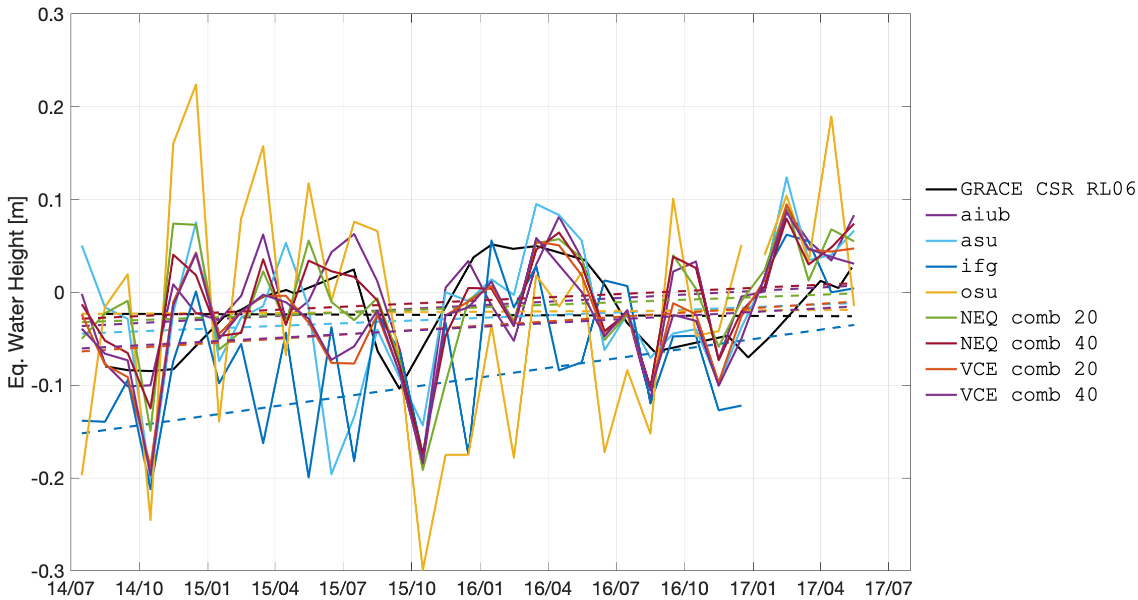

Figure 10 – Time series of EWH for the Mississippi basin (latitude 29 to 44 degrees, longitude -101 to -80 degrees).

solution	constant term [cm]	constant term Δ [cm]	linear term [cm/y]	linear term Δ [cm/year]	corr. coeff. [ ]
GRACE CSR RL06	-2.5	0.0	-0.1	0.0	1.00
aiub	-1.2	1.3	1.5	1.6	0.57
asu	-2.2	0.3	1.2	1.3	0.52
ifg	-7.2	-4.7	4.1	4.2	0.39
osu	-2.0	0.5	0.2	0.2	-0.03
NEQ comb 20	-1.5	1.0	1.1	1.2	0.38
NEQ comb 40	-3.1	-0.6	1.3	1.4	0.57
VCE comb 20	-3.4	-0.9	1.9	2.0	0.60
VCE comb 40	-3.5	-1.1	1.6	1.7	0.60

Table 7 – Statistics of the agreement between the GRACE and Swarm time series for the Mississippi basin.

5.3.5 Columbia region

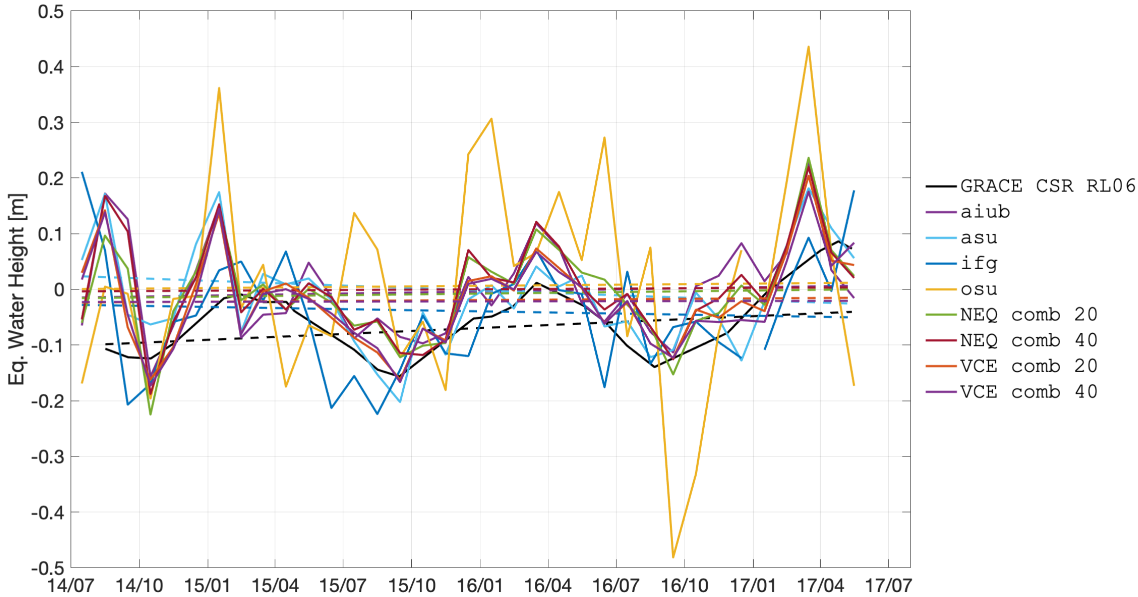

Figure 11 – Time series of EWH for the Columbia region (latitude 38 to 50 degrees, longitude -125 to -110 degrees).

solution	constant term [cm]	constant term Δ [cm]	linear term [cm/y]	linear term Δ [cm/year]	corr. coeff. [ ]
GRACE CSR RL06	-6.2	0.0	2.1	0.0	1.00
aiub	-0.3	5.9	0.7	-1.4	0.34
asu	-1.0	5.1	-1.7	-3.9	0.67
ifg	-4.3	1.8	-0.8	-2.9	0.72
osu	0.8	7.0	0.4	-1.7	0.16
NEQ comb 20	-0.7	5.5	0.6	-1.6	0.62
NEQ comb 40	-0.4	5.8	0.3	-1.9	0.48
VCE comb 20	-1.9	4.3	0.3	-1.8	0.68
VCE comb 40	-2.1	4.0	0.1	-2.1	0.67

Table 8 – Statistics of the agreement between the GRACE and Swarm time series for the Columbia region.

5.3.6 Alaska

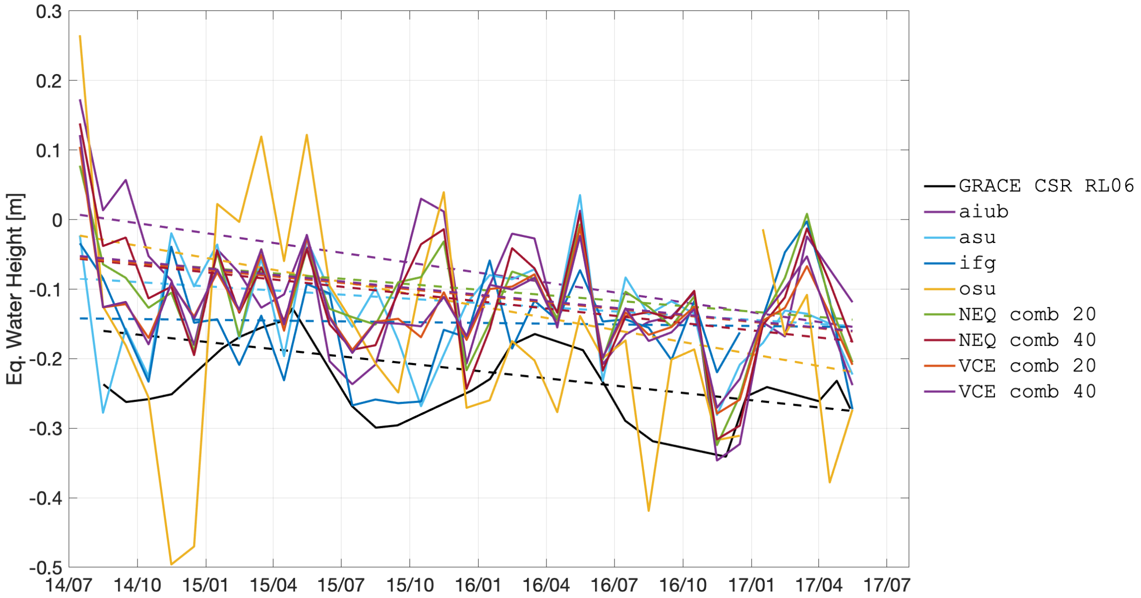

Figure 12 – Time series of EWH for the Alaska (latitude 56 to 65 degrees, longitude -151 to -129 degrees).

solution	constant term [cm]	constant term Δ [cm]	linear term [cm/y]	linear term Δ [cm/year]	corr. coeff. [ ]
GRACE CSR RL06	-23.3	0.0	-4.2	0.0	1.00
aiub	-8.3	15.0	-5.7	-1.5	0.47
asu	-13.2	10.1	-2.4	1.8	0.32
ifg	-15.1	8.2	-0.4	3.8	0.18
osu	-15.8	7.5	-6.9	-2.7	0.66
NEQ comb 20	-10.4	12.9	-3.1	1.0	0.40
NEQ comb 40	-5.0	18.3	-4.2	0.0	0.45
VCE comb 20	-11.4	11.9	-3.7	0.5	0.60
VCE comb 40	-11.2	12.1	-3.8	0.4	0.62

Table 9 – Statistics of the agreement between the GRACE and Swarm time series for the Alaska.

5.3.7 Western Greenland region

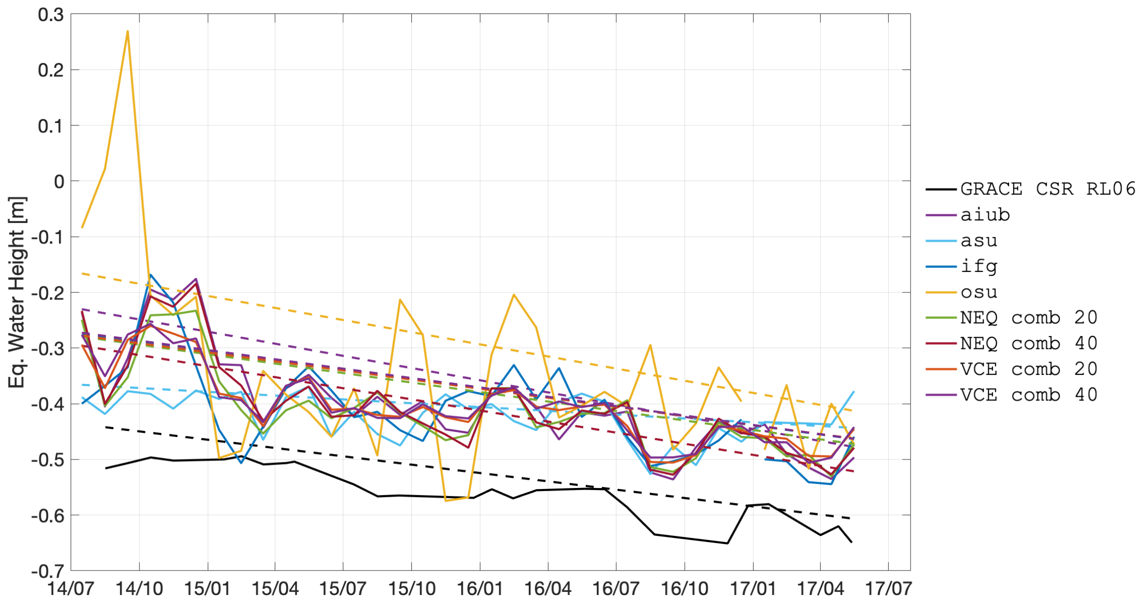

Figure 13 – Time series of EWH for the Western Greenland region (latitude 60 to 85 degrees, longitude -60 to -37 degrees).

solution	constant term [cm]	constant term Δ [cm]	linear term [cm/y]	linear term Δ [cm/year]	corr. coeff. [ ]
GRACE CSR RL06	-54.6	0.0	-6.0	0.0	1.00
aiub	-36.8	17.8	-8.7	-2.8	0.78
asu	-41.9	12.7	-2.7	3.3	0.51
ifg	-40.5	14.1	-6.6	-0.6	0.59
osu	-33.6	21.0	-8.7	-2.7	0.33
NEQ comb 20	-38.7	15.9	-6.8	-0.8	0.68
NEQ comb 40	-28.3	26.3	-8.0	-2.0	0.74
VCE comb 20	-38.1	16.6	-6.5	-0.5	0.77
VCE comb 40	-37.9	16.8	-6.7	-0.7	0.77

Table 10 – Statistics of the agreement between the GRACE and Swarm time series for the Western Greenland region.

5.3.8 Danube basin

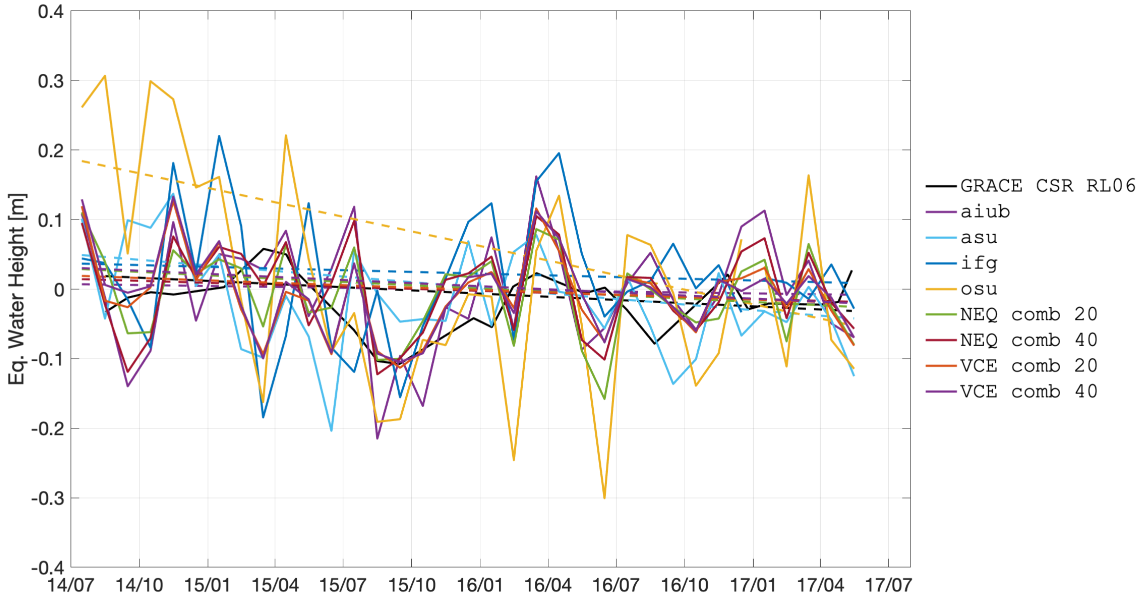

Figure 14 – Time series of EWH for the Danube basin (latitude 43 to 48 degrees, longitude 13 to 28 degrees).

solution	constant term [cm]	constant term Δ [cm]	linear term [cm/y]	linear term Δ [cm/year]	corr. coeff. [ ]
GRACE CSR RL06	-1.3	0.0	-1.8	0.0	1.00
aiub	-0.1	1.2	-0.5	1.3	0.32
asu	-1.4	-0.1	-3.2	-1.4	-0.05
ifg	1.8	3.1	-1.0	0.8	0.04
osu	2.1	3.4	-8.4	-6.5	0.17
NEQ comb 20	-0.1	1.2	-1.9	-0.1	0.15
NEQ comb 40	1.6	2.9	-1.2	0.7	0.27
VCE comb 20	-0.3	1.0	-1.4	0.4	0.13
VCE comb 40	0.2	1.5	-1.8	0.0	0.16

Table 11 – Statistics of the agreement between the GRACE and Swarm time series for the Danube basin.

5.3.9 Western Sub-Saharan basin

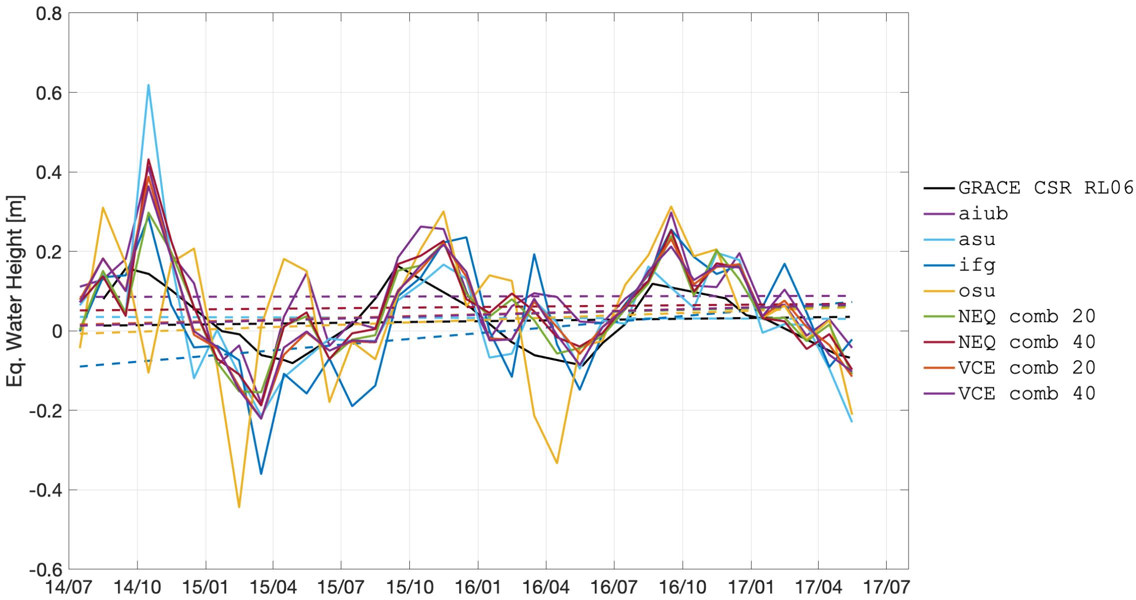

Figure 15 – Time series of EWH for the Western Sub-Saharan basin (latitude 5 to 15 degrees, longitude -15 to -1 degrees).

solution	constant term [cm]	constant term Δ [cm]	linear term [cm/y]	linear term Δ [cm/year]	corr. coeff. [ ]
GRACE CSR RL06	2.7	0.0	0.8	0.0	1.00
aiub	8.7	6.0	0.1	-0.7	0.69
asu	3.2	0.4	-0.2	-1.0	0.70
ifg	2.2	-0.5	5.7	4.9	0.62
osu	3.9	1.1	2.3	1.5	0.33
NEQ comb 20	4.2	1.5	1.6	0.8	0.70
NEQ comb 40	5.1	2.3	0.6	-0.2	0.69
VCE comb 20	4.4	1.6	1.8	1.0	0.74
VCE comb 40	4.2	1.5	1.9	1.1	0.74

Table 12 – Statistics of the agreement between the GRACE and Swarm time series for the Western Sub-Saharan basin.

5.3.10 Eastern Sub-Saharan basin

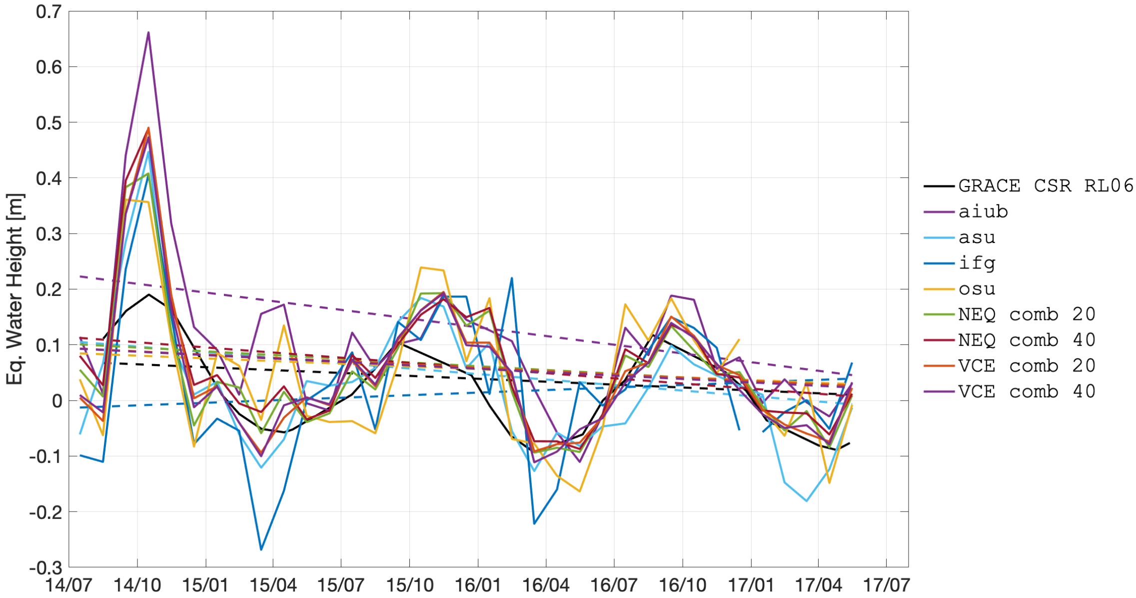

Figure 16 – Time series of EWH for the Eastern Sub-Saharan basin (latitude 1 to 13 degrees, longitude -8 to 35 degrees).

solution	constant term [cm]	constant term Δ [cm]	linear term [cm/y]	linear term Δ [cm/year]	corr. coeff. [ ]
GRACE CSR RL06	3.1	0.0	-2.1	0.0	1.00
aiub	12.4	9.3	-6.3	-4.2	0.68
asu	2.8	-0.3	-3.9	-1.9	0.85
ifg	2.3	-0.8	1.8	3.9	0.62
osu	4.7	1.5	-1.9	0.1	0.66
NEQ comb 20	5.8	2.7	-2.7	-0.6	0.78
NEQ comb 40	11.8	8.7	-3.7	-1.6	0.79
VCE comb 20	5.6	2.5	-2.4	-0.3	0.79
VCE comb 40	5.4	2.3	-2.5	-0.4	0.78

Table 13 – Statistics of the agreement between the GRACE and Swarm time series for the Eastern Sub-Saharan basin.

5.3.11 Congo and Zambezi basins

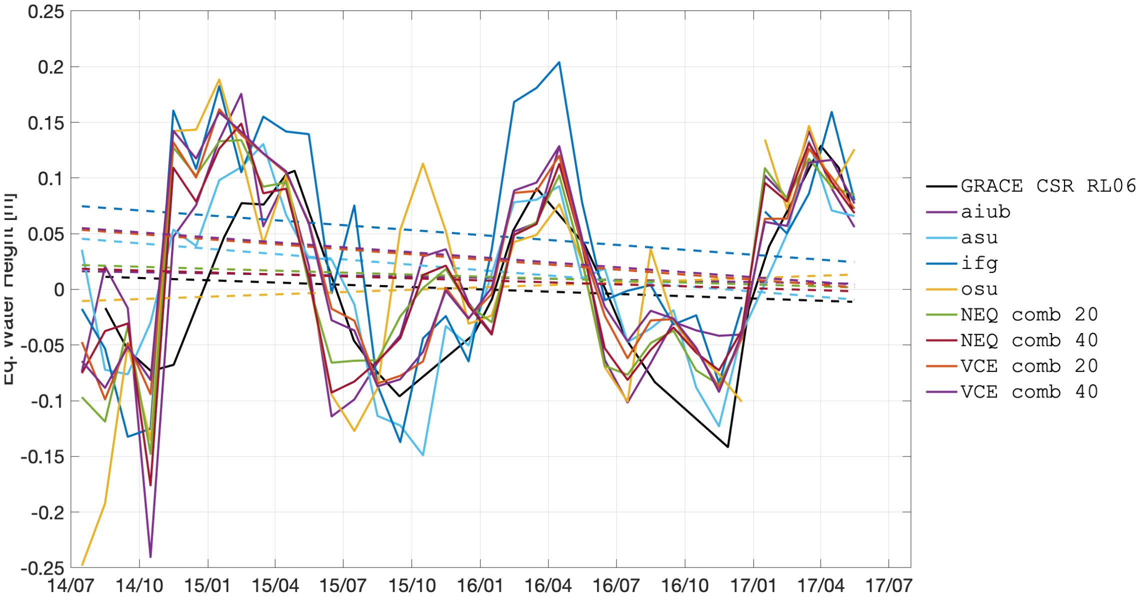

Figure 17 – Time series of EWH for the Congo and Zambezi basins (latitude -23 to -3 degrees, longitude 14 to 38 degrees).

solution	constant term [cm]	constant term Δ [cm]	linear term [cm/y]	linear term Δ [cm/year]	corr. coeff. [ ]
GRACE CSR RL06	-0.3	0.0	-0.8	0.0	1.00
aiub	1.0	1.3	-0.4	0.4	0.74
asu	0.8	1.1	-1.9	-1.1	0.84
ifg	4.0	4.3	-1.8	-1.0	0.77
osu	0.6	0.9	0.8	1.7	0.61
NEQ comb 20	1.1	1.4	-0.7	0.1	0.72
NEQ comb 40	2.0	2.3	-0.7	0.1	0.75
VCE comb 20	2.5	2.8	-1.8	-1.0	0.78
VCE comb 40	2.7	3.0	-1.8	-1.0	0.79

Table 14 – Statistics of the agreement between the GRACE and Swarm time series for the Congo and Zambezi basins.

5.3.12 Volga basin

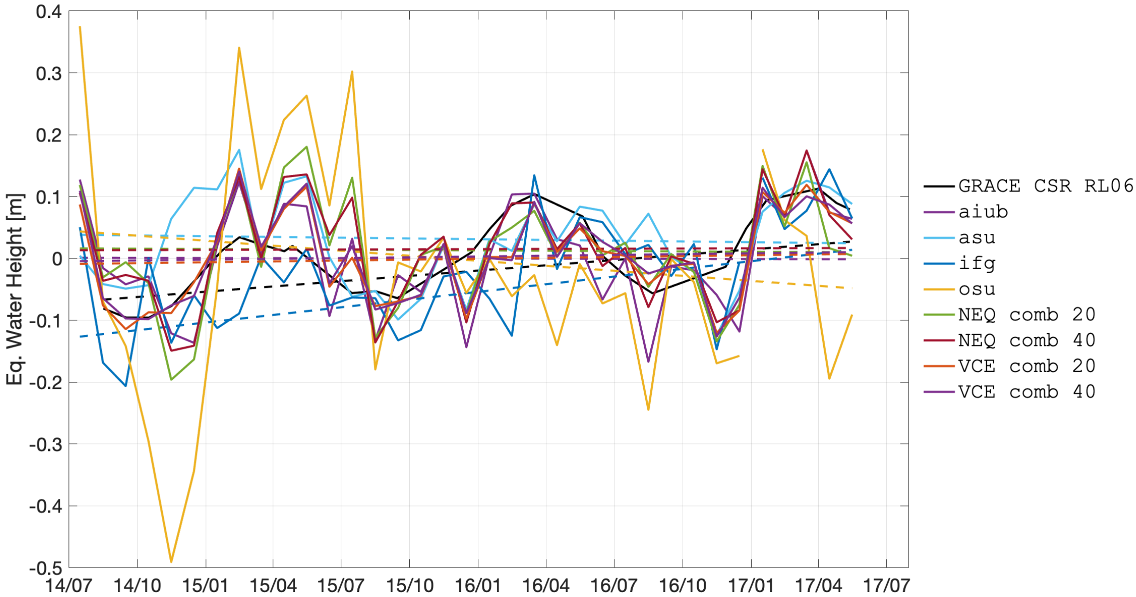

Figure 18 – Time series of EWH for the Volga basin (latitude 53 to 61 degrees, longitude 34 to 56 degrees).

solution	constant term [cm]	constant term Δ [cm]	linear term [cm/y]	linear term Δ [cm/year]	corr. coeff. [ ]
GRACE CSR RL06	-0.7	0.0	3.4	0.0	1.00
aiub	-0.0	0.7	-0.1	-3.5	0.67
asu	2.9	3.6	-0.5	-3.9	0.58
ifg	-3.0	-2.3	5.0	1.5	0.68
osu	-1.9	-1.2	-3.2	-6.7	0.31
NEQ comb 20	1.3	2.0	-0.2	-3.6	0.52
NEQ comb 40	1.3	2.0	0.1	-3.3	0.64
VCE comb 20	0.0	0.7	0.6	-2.9	0.76
VCE comb 40	0.4	1.1	0.5	-2.9	0.75

Table 15 – Statistics of the agreement between the GRACE and Swarm time series for the Volga basin.

5.3.13 Siberia region

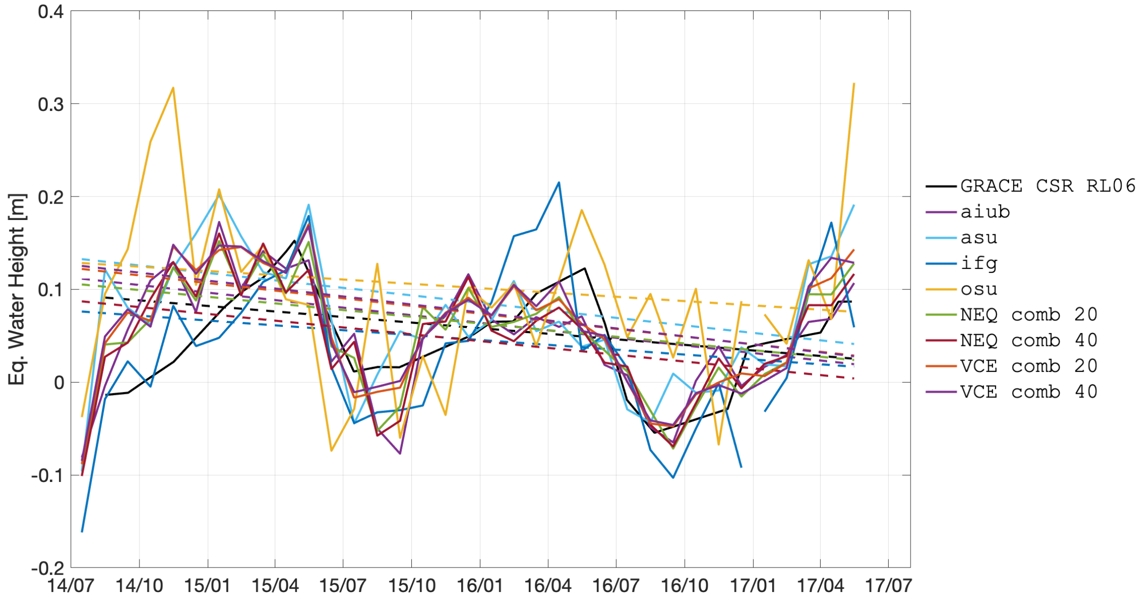

Figure 19 – Time series of EWH for the Siberia region (latitude 57 to 72 degrees, longitude 68 to 109 degrees).

solution	constant term [cm]	constant term Δ [cm]	linear term [cm/y]	linear term Δ [cm/year]	corr. coeff. [ ]
GRACE CSR RL06	5.0	0.0	-2.4	0.0	1.00
aiub	6.0	1.1	-3.3	-0.9	0.63
asu	7.0	2.0	-3.2	-0.8	0.58
ifg	3.5	-1.4	-2.1	0.3	0.73
osu	9.2	4.3	-1.9	0.5	0.21
NEQ comb 20	6.0	1.0	-2.9	-0.5	0.67
NEQ comb 40	9.2	4.2	-2.9	-0.5	0.62
VCE comb 20	7.0	2.1	-3.3	-0.9	0.70
VCE comb 40	7.1	2.2	-3.4	-1.0	0.69

Table 16 – Statistics of the agreement between the GRACE and Swarm time series for the Siberia region.

5.3.14 Ganges-Brahmaputra basin

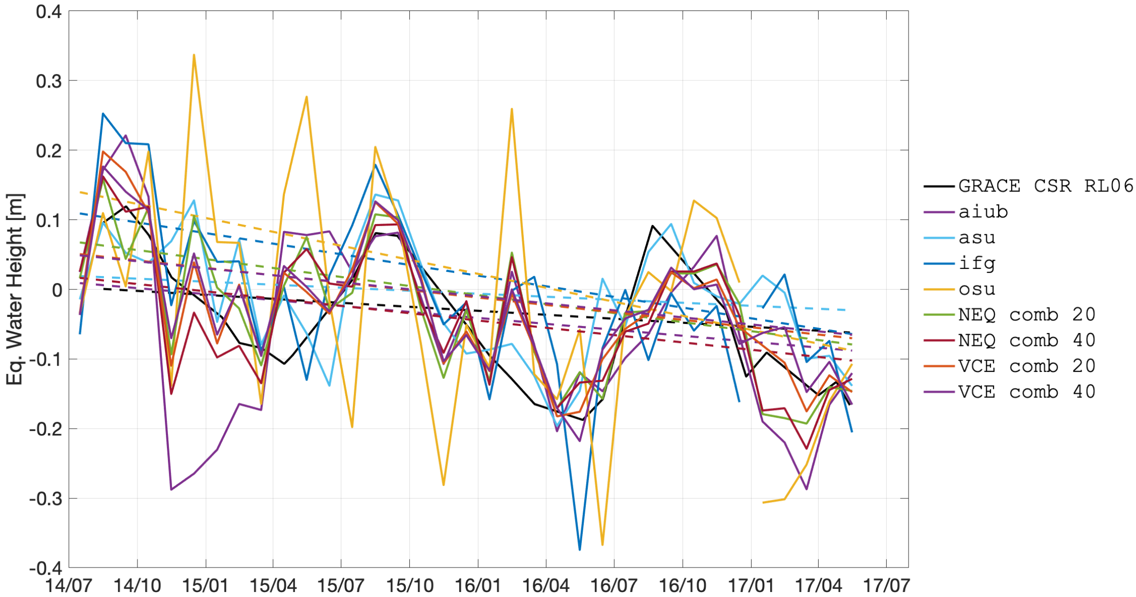

Figure 20 – Time series of EWH for the Ganges-Brahmaputra basin (latitude 15 to 30 degrees, longitude 72 to 89 degrees).

solution	constant term [cm]	constant term Δ [cm]	linear term [cm/y]	linear term Δ [cm/year]	corr. coeff. [ ]
GRACE CSR RL06	-3.9	0.0	-2.3	0.0	1.00
aiub	-4.5	-0.6	-3.4	-1.1	0.58
asu	-1.5	2.4	-1.7	0.6	0.81
ifg	-1.0	2.9	-6.1	-3.8	0.77
osu	-1.7	2.2	-8.0	-5.7	0.44
NEQ comb 20	-1.4	2.5	-5.2	-2.9	0.74
NEQ comb 40	2.3	6.2	-4.2	-1.9	0.71
VCE comb 20	-1.7	2.2	-4.3	-2.0	0.80
VCE comb 40	-1.5	2.4	-4.0	-1.7	0.82

Table 17 – Statistics of the agreement between the GRACE and Swarm time series for the Ganges-Brahmaputra basin.

5.3.15 Indochina region

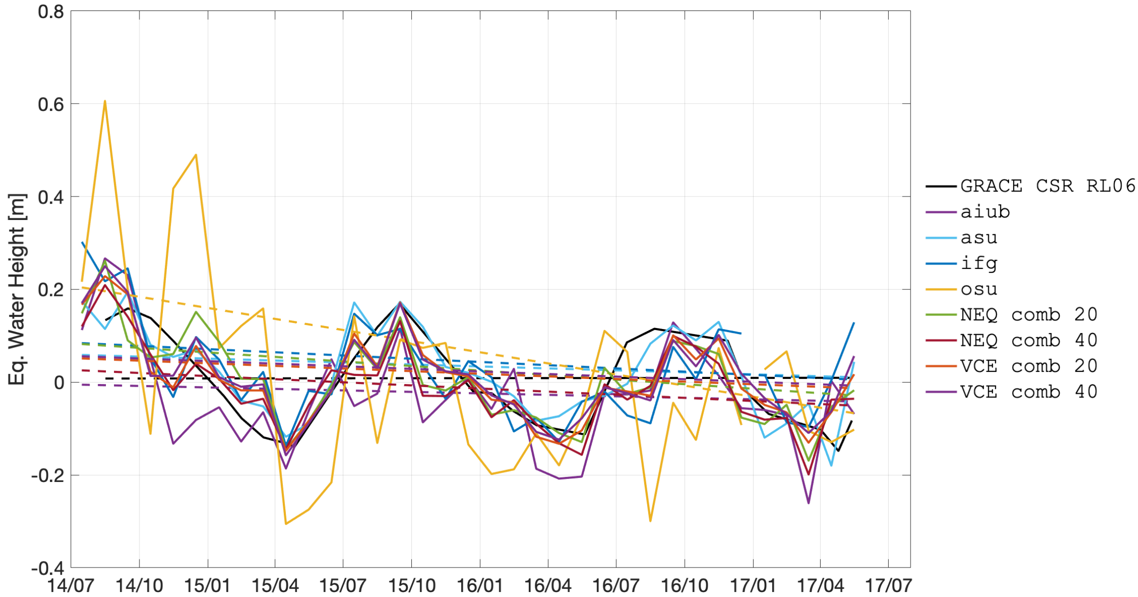

Figure 21 – Time series of EWH for the Indochina region (latitude 12 to 29 degrees, longitude 93 to 105 degrees).

solution	constant term [cm]	constant term Δ [cm]	linear term [cm/y]	linear term Δ [cm/year]	corr. coeff. [ ]
GRACE CSR RL06	0.9	0.0	0.1	0.0	1.00
aiub	-2.6	-3.4	-1.3	-1.3	0.70
asu	2.6	1.7	-1.7	-1.7	0.89
ifg	3.0	2.1	-2.8	-2.8	0.57
osu	1.8	0.9	-9.6	-9.6	0.44
NEQ comb 20	2.1	1.2	-3.9	-4.0	0.74
NEQ comb 40	3.0	2.1	-2.7	-2.7	0.81
VCE comb 20	1.6	0.7	-2.3	-2.3	0.78
VCE comb 40	2.1	1.2	-2.2	-2.3	0.74

Table 18 – Statistics of the agreement between the GRACE and Swarm time series for the Indochina region.

5.3.16 Northern Australia region

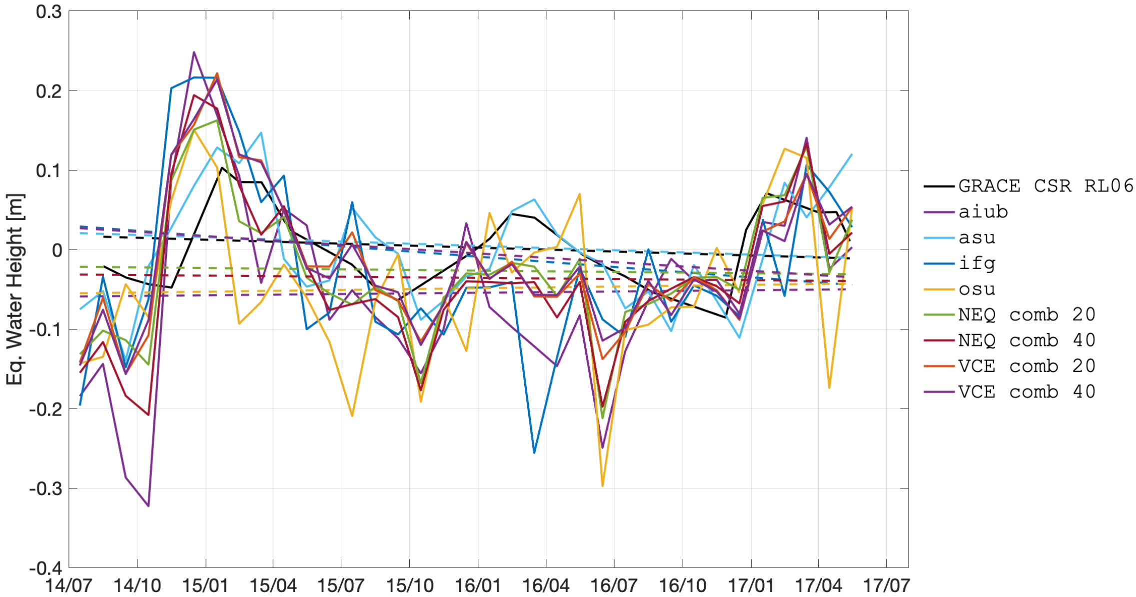

Figure 22 – Time series of EWH for the Northern Australia region (latitude -24 to -10 degrees, longitude 124 to 145 degrees).

solution	constant term [cm]	constant term Δ [cm]	linear term [cm/y]	linear term Δ [cm/year]	corr. coeff. [ ]
GRACE CSR RL06	-0.1	0.0	-1.0	0.0	1.00
aiub	-5.4	-5.3	0.3	1.3	0.53
asu	-0.1	0.0	-1.1	-0.1	0.66
ifg	-2.1	-2.0	-2.6	-1.6	0.45
osu	-4.6	-4.5	0.4	1.4	0.23
NEQ comb 20	-2.7	-2.6	-0.3	0.7	0.62
NEQ comb 40	-3.1	-3.0	-0.3	0.7	0.64
VCE comb 20	-0.7	-0.6	-2.2	-1.2	0.66
VCE comb 40	-0.7	-0.6	-2.2	-1.2	0.66

Table 19 – Statistics of the agreement between the GRACE and Swarm time series for the Northern Australia region.

5.3.17 Western Antarctica region

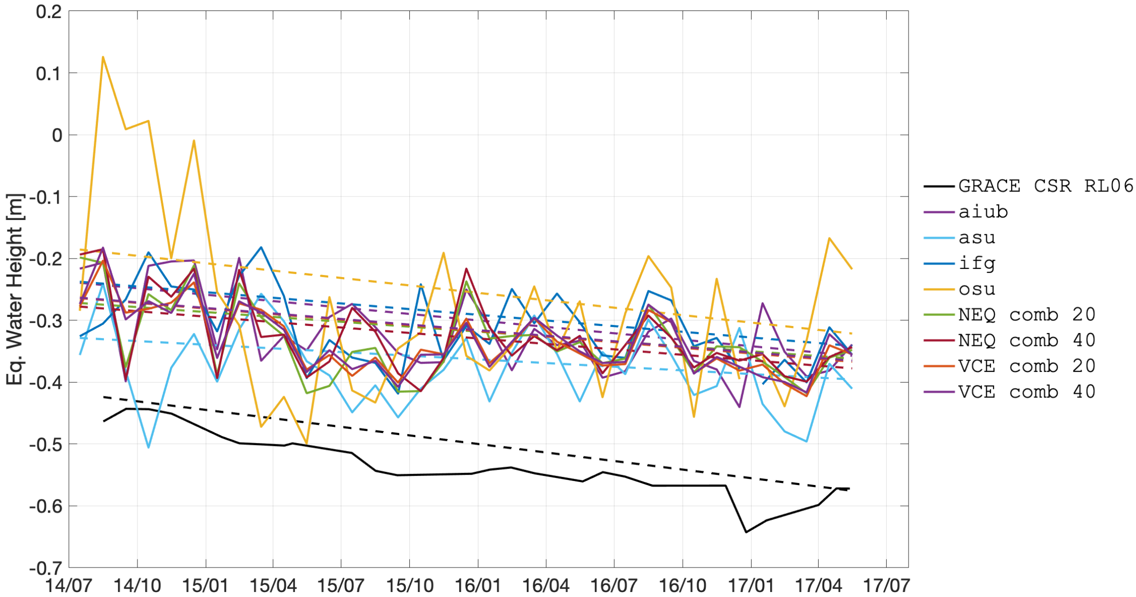

Figure 23 – Time series of EWH for the Western Antarctica region (latitude -80 to -70 degrees, longitude -140 to -85 degrees).

solution	constant term [cm]	constant term Δ [cm]	linear term [cm/y]	linear term Δ [cm/year]	corr. coeff. [ ]
GRACE CSR RL06	-52.0	0.0	-5.5	0.0	1.00
aiub	-30.5	21.5	-4.2	1.4	0.49
asu	-37.5	14.5	-2.4	3.1	0.16
ifg	-30.9	21.1	-3.7	1.9	0.67
osu	-27.9	24.1	-4.8	0.7	0.44
NEQ comb 20	-32.2	19.8	-3.2	2.3	0.46
NEQ comb 40	-27.2	24.8	-3.5	2.0	0.47
VCE comb 20	-32.1	19.8	-3.6	1.9	0.67
VCE comb 40	-32.0	20.0	-3.6	1.9	0.65

Table 20 – Statistics of the agreement between the GRACE and Swarm time series for the Western Antarctica region.

5.3.18 Eastern Antarctica region

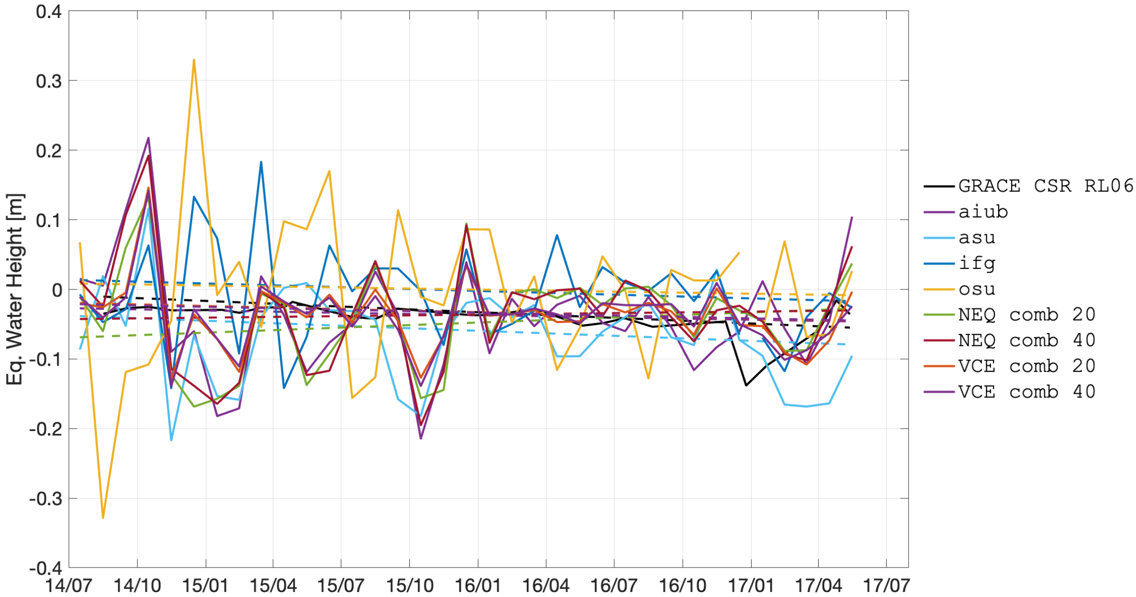

Figure 24 – Time series of EWH for the Eastern Antarctica region (latitude -80 to -68 degrees, longitude 80 to 130 degrees).

solution	constant term [cm]	constant term Δ [cm]	linear term [cm/y]	linear term Δ [cm/year]	corr. coeff. [ ]
GRACE CSR RL06	-3.9	0.0	-1.6	0.0	1.00
aiub	-3.8	0.1	-0.7	1.0	0.06
asu	-6.6	-2.8	-1.4	0.2	0.14
ifg	-0.7	3.1	-1.1	0.6	0.16
osu	-0.3	3.6	-0.6	1.0	0.01
NEQ comb 20	-4.6	-0.7	1.5	3.1	0.08
NEQ comb 40	-4.3	-0.5	0.4	2.1	0.12
VCE comb 20	-3.4	0.5	-0.9	0.7	0.18
VCE comb 40	-3.4	0.4	-0.8	0.8	0.20

Table 21 – Statistics of the agreement between the GRACE and Swarm time series for the Eastern Antarctica region.

5.3.19 Overview

In Sections 5.3.1 to 5.3.18, we illustrate the time series of mean EWH over selected polar regions and major river basins. Generally, the Swarm time series are noisier than GRACE but show a peak-to-peak with comparable amplitude. The Swarm models considering solution-level combination are in better agreement with GRACE than the NEQ-level combination. The agreement of the combined solutions is proportional to the size of the river basin, with Amazon showing excellent agreement, with a correlation coefficient reaching 0.95 and a discrepancy in the trend estimation under 7mm/year. Smaller river basins, such as La Plata and the Mississippi have lower correlation coefficients (as low as 0.13 for the Danube basin) but generally one can expect values above 0.6 for all major river basins. The agreement of the trends derived from the solution-level combination models are generally within 2 cm/year, except for the Indochina regions where it is -2.3 cm/year; they are below 1 cm/year except for La Plata, Mississippi, Columbia, Ganges-Brahmaputra, Western Antarctica, Indochina and Northern Australia regions, where they are -1.7, 1.7, -1.8, -1.7, 1.9 and -1.2 cm/year, respectively. Notably, the trends for the Eastern Antarctica region and Greenland derived from the Swarm solution-level combination are 1cm/year or less relative to GRACE (0.7 and -0.5 cm/year respectively). We do not have an explanation for the large bias between the Swarm and GRACE time series for regions close to the poles where fast ice loss is taking place, i.e. the Greenland, Western Antarctic and Alaska regions.

To better quantify the quality of the various combined Swarm models, the RMS of the constant and linear terms difference w.r.t. GRACE, as well as the mean correlation coefficient are shown in Table 22. The combination at solution level considering VCE weights derived from degree 2 to 20, version 09 (*VCE comb 20*) shows the best overall agreement with GRACE than any other, although only slightly better in bias than combination at solution level considering VCE weights derived from the complete degree range, version 10 (*VCE comb 40*). The combination at the level of NEQ considering VCE weights and empirical factors derived from degree 2 to 20, version 07 (*NEQ comb 20*) comes third, with a higher disagrement in trend and a lower correlation coefficient, although the bias is slightly lower than in case of *VCE comb 40.* We argue that the *NEQ comb 40* has the limitation of representing a large bias discrepancy w.r.t GRACE, larger than all individual models.

Table 22 also illustrates the success of the *VCE comb 20* combination strategy. Of the individual models, only those from ASU and IfG agree better with GRACE in terms of the constant offset: 5.67 and 6.94 vs. 7.03 for *VCE comb 20.* No other statistic or individual model out-performs the *VCE comb 20* combination strategy.

solution	constant term Δ RMS [cm]	linear term Δ RMS [cm/year]	corr. coeff. mean [ ]
GRACE CSR RL06	0.00	0.00	1.00
aiub	8.33	1.78	0.58
asu	5.67	2.02	0.58
ifg	6.94	2.61	0.56
osu	8.20	3.78	0.36
NEQ comb 20	7.05	1.86	0.58
NEQ comb 40	10.36	1.59	0.62
VCE comb 20	7.03	1.43	0.66
VCE comb 40	7.11	1.43	0.66

Table 22 – Statistics of the agreement between the GRACE and Swarm time series for the regions displayed in Sections 5.3.1 to 5.3.18.

5.4 Temporal variability

One interesting aspect of the individual solutions concerns the spatial map of their temporal variability, cf. Figure 25. Note that the colour bars are not in agreement to accentuate the spatial patterns. It is clear that the individual solutions computed with the orbits from IfG (ASU and IfG, bottom row) have quite different variability patterns than the individual solutions compute from AIUB orbits (AIUB and OSU, top row). In the last group, the patterns are vastly different, with AIUB having large variability over the South Pole, to a less extent, the North

Pole and a clear geomagnetic equator signature, while OSU's solutions have high variability spread over a wider latitude range and very small at the Poles. Our combination strategy has successfully mitigated these effects, further demonstrating its success.

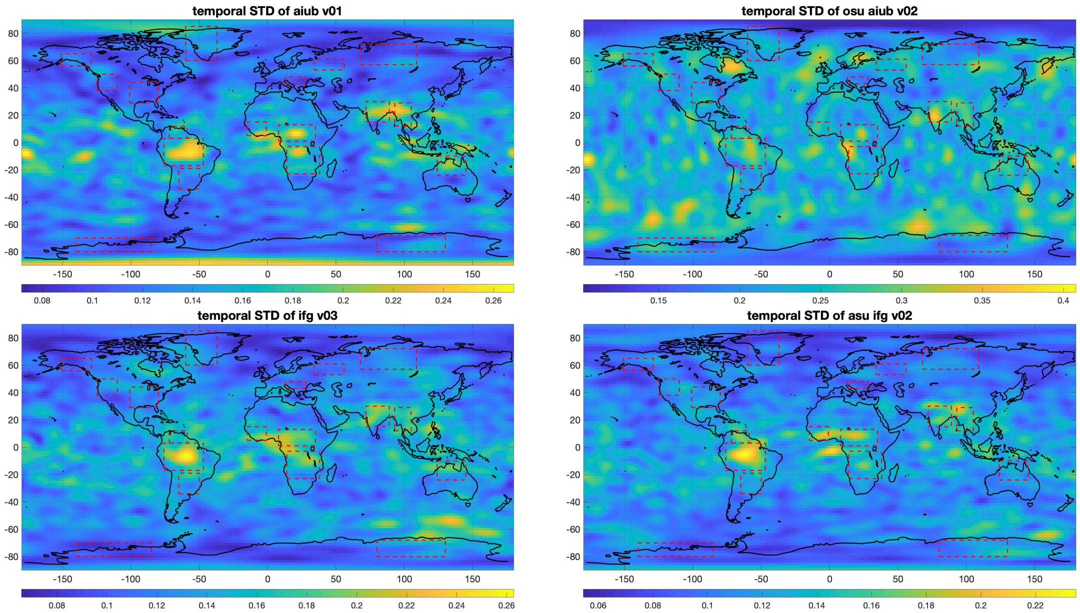

Figure 25 – Temporal variability of the individual solutions

Referring to Figure 26, the spatial patterns of the variability of the combined models is fairly similar between themselves and there is no obvious error pattern (cf. over the oceans) that is clearly represented in any individual solution.

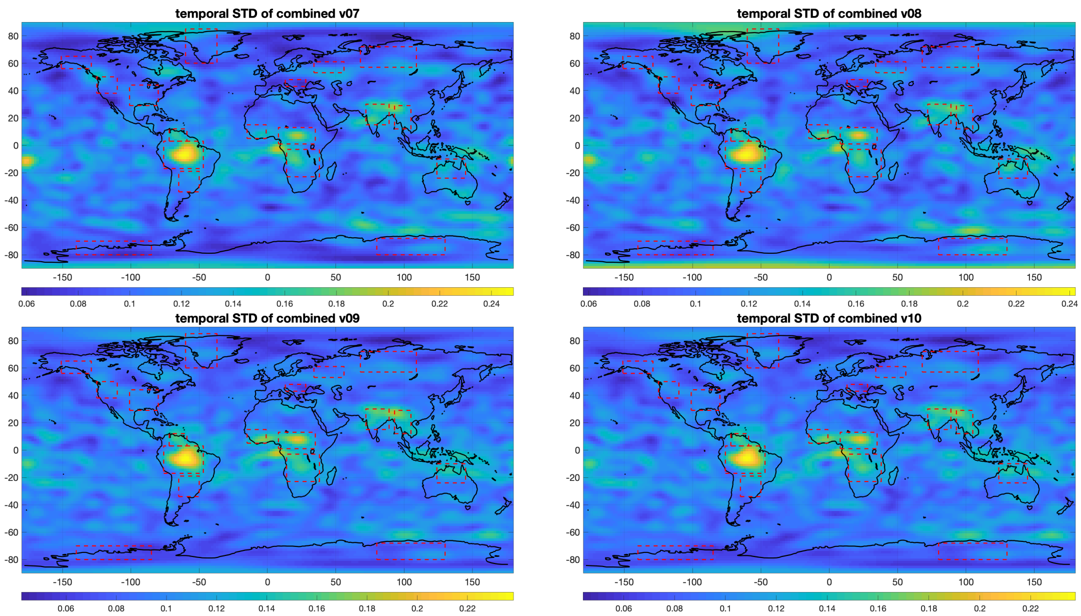

Figure 26 – Temporal variability of the combined solutions

6 Conclusion

We demonstrate that the combined solution, following the *VCE comb 20* strategy, has provided the Swarm-derived gravity field model time series that is in better agreement with GRACE. We do this in terms of spatial and temporal correlations and differences w.r.t. GRACE, both at the global and regional scales. Since GRACE is a dedicated gravimetric mission, its sensitivity and spatial resolution is superior to Swarm. As such, the better agreement of the *VCE comb 20* combined model relates directly to its higher quality.

A Acronyms

AA	Acceleration Approach, Rummel (1979)
AIUB	Astronomical Institute of the University of Bern, Switzerland, `www.aiub.unibe.ch`
ASU	Astronomical Institute (Astronomický ústav), AVCR, Ondřejov, `www.asu.cas.cz/en`
AVCR	Czech Academy of Sciences (Akademie věd České Republiky), Czech Republic, `www.avcr.cz/en/`
CSR	Center for Space Research, UTexas, USA, `www.csr.utexas.edu`
EGSIEM	European Gravity Service for Improved Emergency Management, EU Horizon 2020, `www.egsiem.eu`
EBA	Energy Balance Approach, O'Keefe (1957) and Jekeli (1999)
EWH	Equivalent Water Height
EU	European Union
GFM	Gravity Field Model
GRACE	Gravity Recovery And Climate Experiment, Tapley, Reigber and Melbourne (1996) and Tapley (2004)
IfG	Institute of Geodesy, TUG, Graz, `www.ifg.tugraz.at`
KO	Kinematic Orbit
N/A	Not Applicable
NEQ	Normal Equation
OSU	Ohio State University, `www.osu.edu`
RL06	Release 6
RMS	Root Mean Squared
SH	Spherical Harmonic
TU Delft	Delft University of Technology, Netherlands, `www.tudelft.nl`
TUG	Graz University of Technology, Austria, `www.tugraz.at`
UTexas	University of Texas at Austin, `www.utexas.edu`
USA	United States of America
VCE	Variance Component Estimation
WP	Work Package

References

Beutler, Gerhard et al. (2010). **The celestial mechanics approach: theoretical foundations**. In: *J. Geod.* 84.10, pp. 605–624. DOI: 10.1007/s00190-010-0401-7 (cit. on p. 7).

Bezděk, Aleš et al. (2014). **Gravity field models from kinematic orbits of CHAMP, GRACE and GOCE satellites**. In: *Adv. Sp. Res.* 53.3, pp. 412–429. DOI: 10.1016/j.asr.2013.11.031 (cit. on p. 7).

Bezděk, Aleš et al. (2016). **Time-variable gravity fields derived from GPS tracking of Swarm**. In: *Geophys. J. Int.* 205.3, pp. 1665–1669. DOI: 10.1093/gji/ggw094 (cit. on p. 7).

Cheng, M. K. and J. C. Ries (2016). **Technical Note 07: Monthly estimates of C20 from 5 satellites based on GRACE RL05 models**. Austin, USA. URL: https://podaac.jpl.nasa.gov/gravity/grace-documentation (cit. on p. 9).

Guo, J. Y., X. J. Duan and C. K. Shum (2010). **Non-isotropic Gaussian smoothing and leakage reduction for determining mass changes over land and ocean using GRACE data**. In: *Geophys. J. Int.* 181.1, pp. 290–302. DOI: 10.1111/j.1365-246X.2010.04534.x (cit. on p. 15).

Guo, J. Y. et al. (2015). **On the energy integral formulation of gravitational potential differences from satellite-to-satellite tracking**. In: *Celest. Mech. Dyn. Astron.* 121.4, pp. 415–429. DOI: 10.1007/s10569-015-9610-y (cit. on p. 7).

Jäggi, A. et al. (2016). **Swarm kinematic orbits and gravity fields from 18 months of GPS data**. In: *Adv. Sp. Res.* 57.1, pp. 218–233. DOI: 10.1016/j.asr.2015.10.035 (cit. on pp. 7, 11).

Jäggi, A et al. (2018). **European Gravity Service for Improved Emergency Management (EGSIEM) - from concept to implementation**. In: *submited to Geophys. J. Int.* (Cit. on p. 8).

Jekeli, Christopher (1999). **The determination of gravitational potential differences from satellite-to-satellite tracking**. In: *Celest. Mech. Dyn. Astron.* 75.2, pp. 85–101. DOI: 10.1023/A:1008313405488 (cit. on p. 36).

Mayer-Gürr, Torsten (2006). **Gravitationsfeldbestimmung aus der Analyse kurzer Bahnbögen am Beispiel der Satellitenmissionen CHAMP und GRACE**. PhD thesis. Rheinischen Friedrich-Wilhelms Universität Bonn. URL: http://hss.ulb.uni-bonn.de/2006/0904/0904.pdf (cit. on p. 7).

Meyer, Ulrich, Yoomin Jean and Adrian Jäggi (2018). **Combination of GRACE monthly gravity fields at normal equation level**. In: *Submitt. to J. Geod.* (Cit. on p. 8).

O'Keefe, John A. (1957). **An application of Jacobi's integral to the motion of an earth satellite**. In: *Astron. J.* 62, p. 265. DOI: 10.1086/107530 (cit. on p. 36).

Rummel, R. (1979). **Determination of short-wavelength components of the gravity field from satellite-to-satellite tracking or satellite gradiometry**. In: *Manuscripta Geod.* 4.2, pp. 107–148 (cit. on p. 36).

Shang, Kun et al. (2015). **GRACE time-variable gravity field recovery using an improved energy balance approach**. In: *Geophys. J. Int.* 203.3, pp. 1773–1786. DOI: 10.1093/gji/ggv392 (cit. on p. 7).

Tapley, B., C. Reigber and W Melbourne (1996). **Gravity Recovery And Climate Experiment (GRACE) mission**. Baltimore, USA (cit. on p. 36).

Tapley, B.~D. et al. (2013). **The Status and Future Prospect for GRACE After the First Decade**. In: *AGU Fall Meet. Abstr.* Abstract G32A-01. San Francisco, CA, USA. URL: http://abstractsearch.agu.org/meetings/2013/FM/G32A-01.html (cit. on p. 9).

Tapley, Byron D. (2004). **GRACE Measurements of Mass Variability in the Earth System**. In: *Science (80-.).* 305.5683, pp. 503–505. DOI: 10.1126/science.1099192 (cit. on p. 36).

Teixeira Encarnação, Joao and Pieter Visser (2017). **TN-01 : Standards and Background Models**. Tech. rep. Delft, the Netherlands: Delft University of Technology. URL: http://jgte.github.io/gswarm/TN-01/TN-01.pdf (cit. on p. 7).

Zehentner, Norbert and Torsten Mayer-Gürr (2016). **Precise orbit determination based on raw GPS measurements**. In: *J. Geod.* 90.3, pp. 275–286. DOI: 10.1007/s00190-015-0872-7 (cit. on p. 7).